ROTOR AEROELASTIC STABILITY ASSESSMENT IN THE NEW CORAL FRAMEWORK

Claudio Pasquali, claudio.pasquali@uniroma3.it, Roma Tre University (Italy)
Nikos Spyropoulos, nspyro@fluid.mech.ntua.gr, National Technical University of Athens (Greece)
Riekert Leibbrandt, riekert.leibbrandt@koptergroup.de, Kopter Germany GmbH (Germany)
Massimo Gennaretti, massimo.gennaretti@uniroma3.it, Roma Tre University (Italy)
Vasilis A. Riziotis, vasilis@fluid.mech.ntua.gr, National Technical University of Athens (Greece)
Simon Radler, simon.radler@koptergroup.de, Kopter Germany GmbH (Germany)
Giovanni Bernardini, giovanni.bernardini@uniroma3.it, Roma Tre University (Italy)
George Papadakis, papis@fluid.mech.ntua.gr, National Technical University of Athens (Greece)

Abstract
In the present work, a non-standard procedure for aeroelastic stability assessment of rotors is proposed, it exploits the potentialities of the new multi-fidelity comprehensive rotorcraft simulation tool CORAL. This procedure uses a system identification approach to obtain a data-derived, tridimensional unsteady aerodynamic linearised model to couple with the linearised structural dynamics of the rotor. The linearised aerodynamic model is obtained from suited chirp perturbations of the elastic degrees of freedom of the blade about a steady trimmed solution, followed by a rational approximation of the transfer function matrix, which allows you to account for the aerodynamic hidden states. The rotor structural model is obtained through an analytical linearization of the non-linear multi-body dynamic equations, where the blades are modelled as assemblies of full stiffness matrix Timoshenko beams discretised through FEM elements. Once the linearised aeroelastic system is assembled, it is expressed in a state-space form, and a generalised eigenproblem is solved to evaluate the rotor stability margin. The Sharpe experimental campaign of 1986, dealing with the stability analysis of a hovering rotor, has been chosen as a benchmark for the first validation of the proposed methodology. The experimental lead-lag damping coefficients are successfully compared with numerical ones, computed through the CORAL mid-fidelity Lifting-Line/free-wake aerodynamic solver.

1. INTRODUCTION

Helicopter design is generally a very complex task, all the physical phenomena involved require accurate mathematical modelling in order to be well described and accounted for in the whole design process. To overcome these difficulties and make the design process easier, in the past decades, some comprehensive simulation tools have been developed. Many industries and research centres use multi-fidelity modular codes that allow the simulation and analysis of rotorcraft machines including rotor aeroelastic stability assessment, which is one of the most crucial tasks in helicopter design (to be fulfilled for the whole machine's flight envelope), for which accurate fluid and structural dynamics simulations are necessary.

The rotor aero-elastic behaviour is characterised by an intrinsic periodicity, due to aerodynamics, at the rotor revolution frequency (and its multiples) making in principle the mathematical representation of the blades a non-trivial task (Ref. 1). On the other hand, rotor wake instability, and its persistence beneath the blades, make the three-dimensional effects not negligible when the aerodynamic loads of the blade are evaluated. Different approaches were investigated in the past, some of them predict the unsteady air-loads by coupling thin airfoil theory (Theodorsen-like) with the ONERA dynamic stall equation (Ref. 2, 3), although for performance and trim analysis, they usually couple airfoil theory with a free-wake algorithm based on vortex lattice theory.The unsteady aerodynamics model used for the definition of the aeroelastic operator is a crucial issue: in some papers published in the past some of the authors compared the rotor aeroelastic stability behaviour provided by different-fidelity aerodynamic models, demonstrating that these significantly affect the predicted stability margins (see for instance Ref. 4, 5, 6). In particular, in Reference 5 it is demonstrated that the inaccuracy due to the application of 2D models yields an overestimation of the stability margin. This paper presents the potentialities of the new multi-fidelity comprehensive simulation tool CORAL* in performing the aeroelastic stability analysis of helicopter rotors. The CORAL software integrates all the helicopter's disciplines, except for power systems and avionics, into a single easy-to-adapt user-friendly simulation tool that allows to perform comprehensive analyses of both conventional helicopter configurations and non-conventional VTOL vehicles (Ref. 7, 8). Specifically, the paper proposes a methodology that uses the medium-fidelity solver included in CORAL to perform the aeroelastic stability analysis of helicopter rotors.

The core of the method is in the modelling of unsteady aerodynamics through a Reduced Order Model (ROM) directly derived from a numerical solver. Then, the Rational Matrix Approximation (RMA) of the identified model provides the inclusion of wake and unsteady effects by introducing additional dynamic states that, combined with the rotor degrees of freedom, yield a linearised aeroelastic eigenproblem from which the damping characteristics of the system are easily derived. Data-driven reduced order modelling enables a reduction of the high complexity of the multi-physics interaction, whose simulation requires a relevant computational effort not always compatible with the designer's activities, at the cost of a limited loss of accuracy.

Some of the authors have already demonstrated the potentiality of this kind of approach, for instance, by applying it to main rotor dynamics (Ref. 9), main rotor aerodynamics (Ref. 6) and wake inflow (Ref. 10). In this work, the integration and application of the ROM/RMA for aeroelastic purposes in the CORAL design suite will be deeply described and applied. Even if already implemented in CORAL for rotors in forward flight conditions, here the proposed approach is applied to a hovering rotor, and its capabilities are tested by comparing the numerically evaluated damping coefficients of the two-bladed hovering rotor studied by Sharpe (Ref. 11) with those experimentally acquired. The Sharpe rotor is a small-scale hingeless rotor specifically built to validate aeroelastic codes, the blades have relatively low torsional stiffness to emphasise its influence in flap-lag-torsion coupling and the hub is designed to allow variations in pre-cone and droop angle, which are two parameters that may severely change the rotor aeroelastic stability characteristics.

The paper is structured as follows: in the Section 2, the proposed procedure to evaluate rotor aeroelastic stability is outlined; in Section 3, the Rational Matrix Approximation method is pointed out; in Section 4, the CORAL aeroelastic solver capabilities are described and in Section 5 the obtained results presented. Finally, in Section 6, the outcomes of this work are collected.

*The CORAL project involves partners in Italy (Roma Tre University), Greece (National Technical University of Athens and the consulting company iWind) and Canada (Carleton University's Rotorcraft Research Group – CU) under the coordination of Kopter Germany, a member of the Leonardo Group.

2. THE METHODOLOGY

The core of the proposed method can be summarised in the following steps:

- evaluation of the steady trimmed solution in a given flight condition;
- identification of the unsteady aerodynamic frequency response (FR) to arbitrary perturbations of the elastic degrees of freedom (and/or hub kinematic variables and pilot inputs);
- least square rational matrix approximations of the FR and transformation into the time domain making explicit the aerodynamic hidden states, $\boldsymbol{\zeta}$;
- coupling this aerodynamic model with the linearised structural dynamic one obtaining the general form: $\dot{\mathbf{z}} = \mathbf{A}\mathbf{z}$, where $\mathbf{z}$ is a vector collecting all the elastic variables and the aerodynamic hidden states.

It is worth noting that for hovering rotors and rotors in axial flight, the linearised aeroelastic system is naturally composed of constant-coefficient equations, whereas for rotors in forward flight, this is obtained through multi-blade transformation followed by constant-coefficient approximation: this is a widely accepted procedure which yields a standard eigenproblem to be examined for the stability analysis (aeroelastic poles are typically characterised as of regressive, progressive and collective type, due to their examination in the non-rotating frame). If the constant-coefficient approximation is not applied, the stability analysis requires the application of the Floquet theory, which is more time-consuming than the standard eigenproblem solution and provides only damping of the dynamic poles, leaving undefined their phases.

In this paper, for the sake of simplicity, the application of the method will be restricted to only hovering rotors, future work will apply the method to forward flight rotors. Considering the perturbed aeroelastic model one has:

(1) $$\mathbf{M}\ddot{\mathbf{q}} + \mathbf{C}\dot{\mathbf{q}} + \mathbf{K}\mathbf{q} = \mathbf{f}_{\text{aer}}$$

where $\mathbf{M}$, $\mathbf{C}$ and $\mathbf{K}$ are the linearised structural mass, damping and stiffness matrices† obtained by a finite element solver and $\mathbf{q}$ and $\mathbf{f}_{\text{aer}}$ are, respectively, the elastic perturbed degrees of freedom and aerodynamic perturbed forces and moments defined in a rotating frame of reference. Then, defining and solving the eigenproblem of $\mathbf{M}^{-1}\mathbf{K}$, which gives back the approximated natural modes of vibration for the rotating beam, and projecting Eq. (1) onto these functions, or more precisely a suitable selection of the lowest frequency ones, one has:

$$\hat{\mathbf{M}}\ddot{\mathbf{q}}_G + \hat{\mathbf{C}}\dot{\mathbf{q}}_G + \hat{\mathbf{K}}\mathbf{q}_G = \mathbf{Z}^T\mathbf{f}_{aer} \tag{2}$$

where:

$$\begin{aligned} \hat{\mathbf{M}} &= \mathbf{Z}^T\mathbf{M}\mathbf{Z} \\ \hat{\mathbf{C}} &= \mathbf{Z}^T\mathbf{C}\mathbf{Z} \\ \hat{\mathbf{K}} &= \mathbf{Z}^T\mathbf{K}\mathbf{Z} \end{aligned} \tag{3}$$

which are square matrices of dimension $[N_{mode} \times N_{mode}]$, where, denoting with N_{fem} the number of FEM degrees of freedom and N_{mode} the number of the selected natural modes of vibration, $N_{mode} << N_{fem}$.
Finally, recalling the Coleman multi-blade transformation [and by applying a time-invariant approximation in the case of footnote †], it is possible to rewrite the system of Eq. (2) in a time-invariant form in a non-rotating frame of reference:

$$\hat{\mathbf{M}}^0_M\ddot{\mathbf{q}}_M + \hat{\mathbf{C}}^0_M\dot{\mathbf{q}}_M + \hat{\mathbf{K}}^0_M\mathbf{q}_M = \mathbf{T}^{-1}\mathbf{Z}^T\mathbf{f}_{aer} \tag{4}$$

where:

$$\begin{aligned} \hat{\mathbf{M}}^0_M &= mean(\mathbf{T}^{-1}\hat{\mathbf{M}}\mathbf{T}) \\ \hat{\mathbf{C}}^0_M &= mean(\mathbf{T}^{-1}(\hat{\mathbf{C}} + 2\hat{\mathbf{M}}\dot{\mathbf{T}})\mathbf{T}) \\ \hat{\mathbf{K}}^0_M &= mean(\mathbf{T}^{-1}(\hat{\mathbf{M}}\ddot{\mathbf{T}} + \hat{\mathbf{C}}\dot{\mathbf{T}} + \hat{\mathbf{K}})\mathbf{T}) \end{aligned} \tag{5}$$

$\mathbf{T}$ is the Coleman transformation matrix and $\mathbf{q}_M$ is a vector collecting the multi-blade, modal:

$$\boldsymbol{q}_M = \boldsymbol{T}\boldsymbol{q}_G \tag{6}$$

Thus, the multi-blade variables of the *k-th* mode can be expressed as:

$$\begin{aligned} q_{0-k}(t) &= \frac{1}{N}\sum_{i=1}^{N} q^i_{G-k}(t) \\ q_{c-k}(t) &= \frac{2}{N}\sum_{i=1}^{N} q^i_{G-k}(t)cos(\Psi_i(t)) \\ q_{s-k}(t) &= \frac{2}{N}\sum_{i=1}^{N} q^i_{G-k}(t)sin(\Psi_i(t)) \\ q_{N/2-k}(t) &= \frac{1}{N}\sum_{i=1}^{N} q^i_{G-k}(t)(-1)^i \end{aligned} \tag{7}$$

where N is the number of rotor blades and $\Psi_i = \Omega t + 2\pi i/N$ is the azimuthal position of the *i-th* blade.

3. REDUCED ORDER MODEL

Once the system has been formulated as in Eq. (5), an arbitrary chirp perturbation of each multi-blade, modal variable about its steady state will be performed and the corresponding generalised perturbed forces $\boldsymbol{f}_M = \mathbf{T}^{-1}\mathbf{Z}^T\mathbf{f}_{aer}$ evaluated through the aerodynamic solver. Then, by using the identification tool Qopter (Ref. 8, 12), which is already integrated into the CORAL design suite, the frequency response matrix representing the unsteady aerodynamics can be identified and then approximated and expressed as explained in the following.
The identified perturbed aerodynamic forces, $\mathbf{f}_M$, are expressed in the frequency-domain as

$$\tilde{\mathbf{f}}_M = \mathbf{H}\,\tilde{\mathbf{q}}_M \tag{8}$$

once the frequency response matrix is suitably sampled in the range of frequency of interest, the application of a least-square procedure yields its following rational-matrix approximation, RMA (Ref. 12),

$$\mathbf{H} = s^2\mathbf{A}_2 + s\mathbf{A}_1 + \mathbf{A}_0 + \mathbf{C}[s\mathbf{I} - \mathbf{A}]^{-1}\mathbf{B} \tag{9}$$

where $\mathbf{A}_2$, $\mathbf{A}_1$, $\mathbf{A}_0$, $\mathbf{A}$, $\mathbf{B}$ and $\mathbf{C}$ are, in principle, real, fully populated matrices and s denotes the Laplace-domain variable (the maximum degree of the polynomial contribution to $\mathbf{H}$ can vary depending on the specific input and outputs involved in the examined problem). Matrices $\mathbf{A}_2, \mathbf{A}_1$ and $\mathbf{A}_0$ are square matrices of dimension $M = (N_{blade} \times N_{mode})$, $\mathbf{A}$, is a $[P \times P]$ matrix containing the P poles of the rational expression, $\mathbf{B}$, is a $[P \times M]$ matrix and $\mathbf{C}$ has dimensions $[M \times P]$. Finally, combining Eq. (8) with Eq. (9) and transforming into the time domain, one obtains

†In the general formulation (*i.e.*: for all flight condition except for hovering and axial flight) those are time dependent matrices.

the following differential model that describes the system dynamics forced by an arbitrary set of inputs, through a finite number of states

$$\begin{cases} \mathbf{f}_{\mathrm{M}} = \mathbf{A}_2 \ddot{q}_M + \mathbf{A}_1 \dot{q}_M + \mathbf{A}_0 q_M + \mathbf{C}\boldsymbol{\zeta} \\ \dot{\boldsymbol{\zeta}} = \mathbf{A}\boldsymbol{\zeta} + \mathbf{B}\mathbf{q}_M \end{cases} \tag{10}$$

where $\boldsymbol{\zeta}$ is the vector of the aerodynamic hidden states introduced by the poles of the approximated transfer function matrix. Using Eq. (10), Eq. (4) can be rewritten:

$$\begin{cases} (\hat{\mathbf{M}}^0_M - \mathbf{A}_2)\ddot{\mathbf{q}}_M + (\hat{\mathbf{C}}^0_M - \mathbf{A}_1)\dot{\mathbf{q}}_M + \\ +(\hat{\mathbf{K}}^0_M - \mathbf{A}_0)\mathbf{q}_M - \mathbf{C}\boldsymbol{\zeta} = 0 \\ \\ \dot{\boldsymbol{\zeta}} = \mathbf{A}\boldsymbol{\zeta} + \mathbf{B}\mathbf{q}_M \end{cases} \tag{11}$$

The system expressed as in Eq. (11) can be easily reduced to its first-order representation, and the corresponding eigenproblem solved to obtain the damping coefficient of the rotor.

4. HIGH FIDELITY AEROELASTIC SOLVER

This section briefly describes the possible aeroelastic solving combination available in the CORAL design suite, it handles the aerodynamic and structural systems separately but solves them tightly coupled. There are several aerodynamic options of varying fidelity available. The lowest fidelity option, with minimum computational requirements but sufficiently reliable in simple flow configurations, is a simplified Blade Element Momentum method (BEM) model enhanced with engineering tools in order to account for the dynamic behaviour of the wake induction (Pitt-Peters-like). In a more elaborate option, the aerodynamic modelling of the blades is based on panel formulations, whereas the wake is handled in a hybrid Free Vortex Wake (VFW) approach (Ref. 13).

Concerning the blade modelling, there are multiple options available, namely: i) the standard Lifting Line (LL) model introduced by Prandtl (Ref. 14, 15); ii) a Lifting Surface (thin) approach where the blade is discretised in panels along its camber surface and for each panel, the potential value jump is calculated by solving the no-penetration condition on its control point (Ref. 16) and iii) a 3D panel representation of the actual blade geometry (thick) by following the direct formulation of Morino (Ref. 17). Regarding the rotor wake modelling, the near-wake part is emitted by the blades as vortex filaments forming lattice and then it is converted into vortex blobs in the far-wake region, enhancing the wake deformability and reducing the Biot-Savart operations and thus accelerating the simulation. In this way, complex flow phenomena may be handled with greater accuracy, however, the flow-field representation is essentially potential, which means that load-driving conditions related to compressibility and viscous effects (such as stall-induced effects) are not accounted for. For this reason, *a-posteriori* compressible and viscous corrections are applied on the blade loads by following a blade element analysis, supplemented with an extended ONERA dynamic stall model as described in Reference 18. The highest fidelity aerodynamic option in CORAL is a 2nd-order compressible finite volume CFD solver (Ref. 19).

In order to investigate the interaction between the rotating blades and stationary bodies (e.g. helicopter fuselage), the Actuator Line (AL) (Ref. 20) modelling of the blades may be employed, which simplifies multi-body configurations and restrains computational cost. However, in cases where flow phenomena related to the actual blade geometry (e.g.: flow separation, shock waves) are to be investigated, the actual geometry of the rotor blades is resolved and multi-body configurations (interaction between arbitrarily moving bodies) are realised through an over-set grid methodology (Ref. 21).

Finally, a hybrid CFD solver is available (Ref. 22) that employs a domain decomposition approach, like overset methodologies do, in order to combine an Eulerian approach close to solid–wall boundaries with a Lagrangian one for the rest of the domain. The flow field in the Lagrangian sub-domain is represented by solving the compressible Navier-Stokes equations under a Vorticity-Dilatation formulation in material coordinates. In this way, accuracy is enhanced, as the true far-field boundary conditions are satisfied and the wake structures are better preserved thanks to the reduced numerical diffusion of the Lagrangian–Vorticity formulation. In order to reduce the computational cost, the Particle Mesh (PM) technique (Ref. 23) is employed for the evaluation of the material derivatives of the Lagrangian particles.

Rigid body and elastic motion due to structural flexibility are concurrently accounted for within a multi-body dynamics framework, alongside the non-linear inertial and structural effects and geometric couplings imposed by large deflections of highly flexible components (blades). These highly flexible components are approximated as assemblies of linear 1D full stiffness matrix Timoshenko beams (Ref. 24) (sub-bodies) discretised through FEM elements. The interconnected linear sub-bodies are linked through proper non-linear kinematic and dynamic compatibility equations. In this way, non-linear geometric and aeroelastic effects due to high deformation are accounted for using linear beam theory at the sub-body level but considering non-linear effects at the connection points (Ref. 25), then, the non-linear multi-body dynamic equations are analytically linearised and expressed in the form of Eq. (1), which facilitates the ROM analysis that follows. Proper kinematic compatibility equations may be used in cases of soft joint modelling, where the extra spring and damper forces are considered. In this manner, flexible beams may be modelled as stiff or uniform mass/stiffness beams with lumped properties integrated into hinge positions.

5. NUMERICAL RESULTS

As mentioned above, the goal of the numerical investigation is to compare the results of the aeroelastic analysis of the hovering Sharpe two-bladed rotor performed within the CORAL design suite and the experimental results obtained by Sharpe (Ref. 11), the main characteristics of the rotor are summarised in Tab. 1.

In the current application, the rotor blades are

Rotor diameter	1.923m
Blade length	0.87m
Hub offset	0.091m
Chord	0.0864m
Airfoil	NACA 0012
Re_{tip}	600,000

Table 1: Sharpe two-bladed, untapered, untwisted rotor main characteristics.

modelled as cantilever beams, the drive-train is assumed to be significantly stiffer than the blades and, thus, is omitted from the computational model. The elastodynamic response of the rotor blades is evaluated by the high fidelity structural dynamics solver (Ref. 20) described in Sec. 4 that models beam-structured configurations under a monodimensional Finite Element Method (FEM). The blades are attached to a revolute joint at the hub radius and a torsional hinge is considered with a spring stiffness of 41.21 Nm/rad to represent the soft link case of the Sharpe work. Then, to constrain the computational cost without losing accuracy, the so-modelled structure has been coupled with the LL (Lifting-Line) aerodynamic solver, the near wake is described as a vortex lattice, which is preserved in this form for four rotor revolutions and, after that, the wake panels are transformed into vortex blobs (particles) to model the far wake region. In order to speed up the simulation, in the passage from the vortex lattice to particles, four adjacent panels are merged into a single vortex particle. To the same aim, particles that are older than eight rotor revolutions are assumed to be adequately away from the rotor plane to consider their downwash as negligible and exclude them from the computational procedure (see Fig. 1).

The first step of the process was the verification

Vibration mode	Experimental (Hz)	CORAL(Hz)
First flap	5.22	5.21
First lag	23.79	22.85
Second flap	30.05	32.54
First torsion	45.89	43.10

Table 2: Main vibration mode frequencies (non-rotating), comparison between experimental and numerical data.

of the rotor structural model comparing the experimental data both in terms of natural vibration modes frequencies of the non-rotating blade and Campbell diagram. Table 2 collects the comparison with the experimental non-rotating frequencies; four modes are considered: first and second flapping, first lead-lag and first torsion, for the no-pitch, no-precone and no-droop blades, whereas Fig. 2 shows the Campbell diagram of the analysed rotor. It is worth noting that the predicted variation of the natural frequencies of the system with the rotational speed is in good agreement with the experimental measured one.

The following step is the evaluation of the aeroelastic equilibrium, Fig. 3 and Fig. 4 depict the results concerning the trimmed conditions, in particular, Fig. 3 shows the three blade moments experimentally measured as a function of the collective

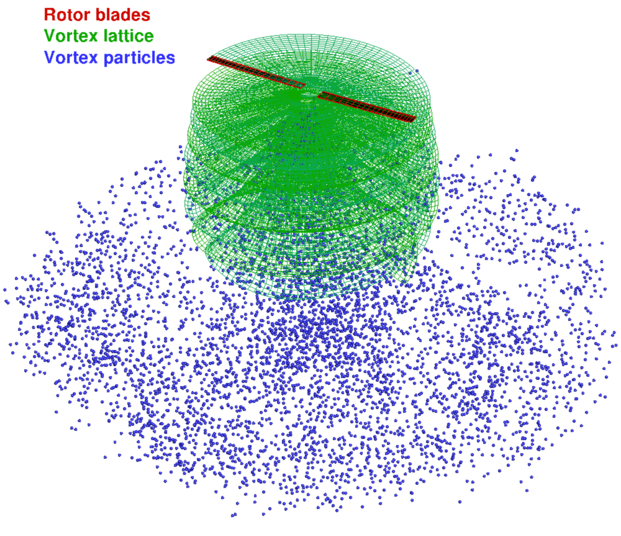

Figure 1: Visualisation of the discretised aerodynamic domain, the blade, the near wake and the wake-blob.

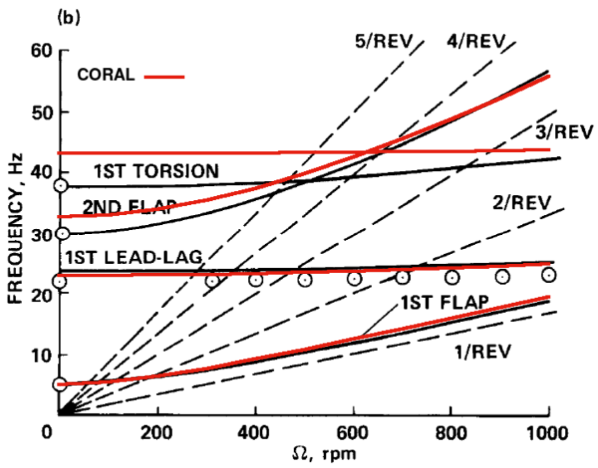

Figure 2: Campbell diagram of the blade natural frequencies from 0 to 1000rpm; black lines are from Sharpe work numerical prediction, empty dots the experimental frequencies and red lines are CORAL results.

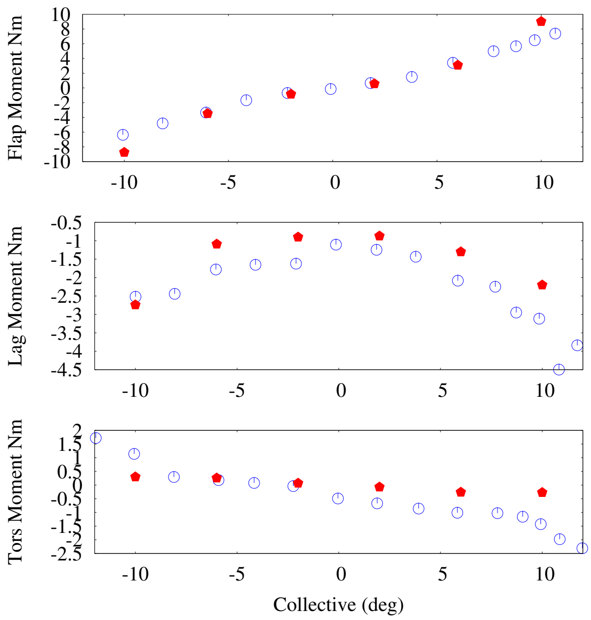

Figure 3: Comparisons of flap, lag and torsion moments *Vs* θ_C; blue empty dots are for experimental results, filled red polygons the CORAL simulated ones.

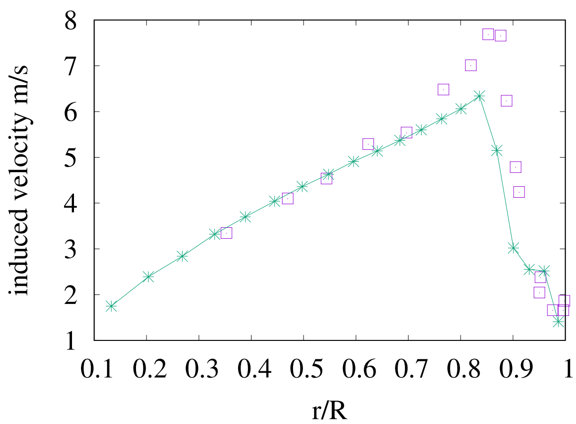

Figure 4: Comparison of the induced velocity over the blade, collective angle, $\theta_c = 6°$; magenta empty dots are for experimental results, filled green the CORAL simulated ones.

pitch angles, compared to the numerically evaluated ones. The figure proves the capability of the aeroelastic solver to well capture both the loads and their dependency on the pitch angle, the more relevant differences can be seen in torsion moment, in particular for high pitch angles. Figure 4 shows the induced velocity over the blade for a pitch angle of $\theta_C = 6°$, it shows a good overall agreement with the experimental data, thus confirming the capability of the proposed aeroelastic solver to capture the main characteristic of the analysed configuration.

Once the fidelity of the rotor aeroelastic model has been assessed, by exploiting the Qopter capabilities, the Rational-Matrix Approximation of the unsteady aerodynamic loads can be obtained starting from adequate chirp perturbation of the modal, non-rotating, degrees of freedom of the system. Several pitch angles are analysed from 0° to 12°, to assess the aeroelastic stability of the rotor in different configurations and verify the robustness of the proposed method. An important outcome of the identification process is the transfer function coherence (Ref. 26), recalling that it is a function measuring the linearity of the considered input/output couple[‡], hence an estimator of the reliability of the identified transfer function in the whole considered frequency domain. Fig. 5 represents an overall measure of the quality of the identified model, it is a condensed representation of the integral coherence evaluated with the following expression (Ref. 27):

$$I = -\frac{1}{2\pi}\int_{f_1}^{f_2} ln(1-\lambda^2(f))df \qquad (12)$$

where λ^2 is the coherence of the considered transfer function. The columns are the output of the system, the generalised forces in the non-rotating frame (collective and differential), and the rows are the inputs, modal deflections in the non-rotating frame, the higher the number in the cell the higher the coherence in the whole considered frequency

[‡]It can vary from 0, no-linear dependence, to 1 full linear dependence; it is commonly considered 0.6 as a threshold value to consider the identified transfer function accurate.

range. To better understand the matrix of Fig. 5, the number in cell $1-1$ is the condensed information coming from the curve in the upper picture of Fig. 6 (which depicts the coherence as a frequency function for two TFs), whereas cell $2-1$ is the result of the integral of the lower one in Fig. 6. Figure 5 suggests that the aerodynamic transfer matrix is block diagonal as expected, thus the collective perturbations do not influence the differential loads and *viceversa*.

Once verified the linearity of the relations, and as-

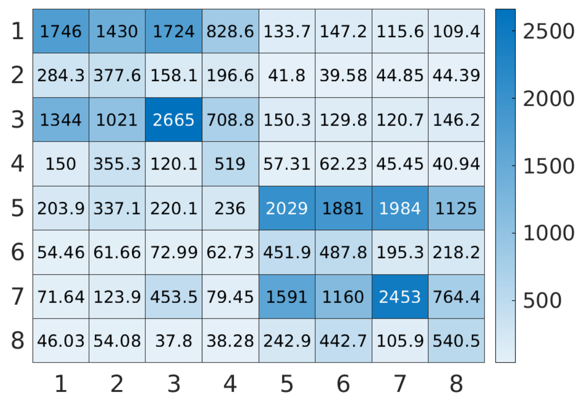

Figure 5: Integral coherence, load-case $\theta = 6°$.

sessed the quality of the identification, the Rational Matrix Approximation of the aerodynamic transfer matrix has been performed. Before coupling the so-obtained unsteady aerodynamic with the linearised structural system, the RMA has been validated by comparing the response of the system to an arbitrary input with the one obtained for the same input through the LL, free-wake solver. Considering for in-

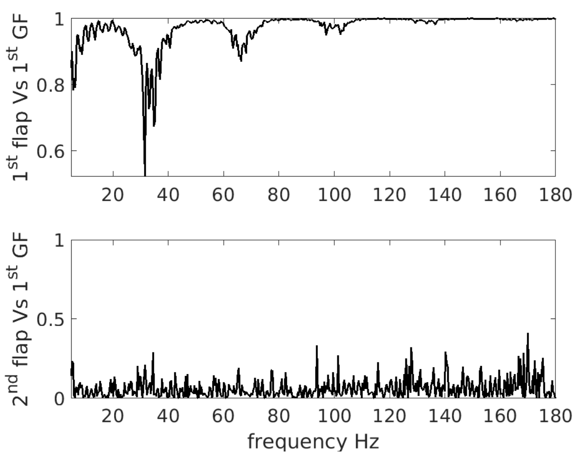

Figure 6: Transfer function's coherence, load-case $\theta = 6°$.

stance the arbitrary first flapping collective mode perturbation around $\theta_C = 6°$, Fig. 7 shows the input and the corresponding output, the first generalised collective force, a very good agreement is observed between the aerodynamic solver (blue line) and its reduced-order representation (red line). Finally, the

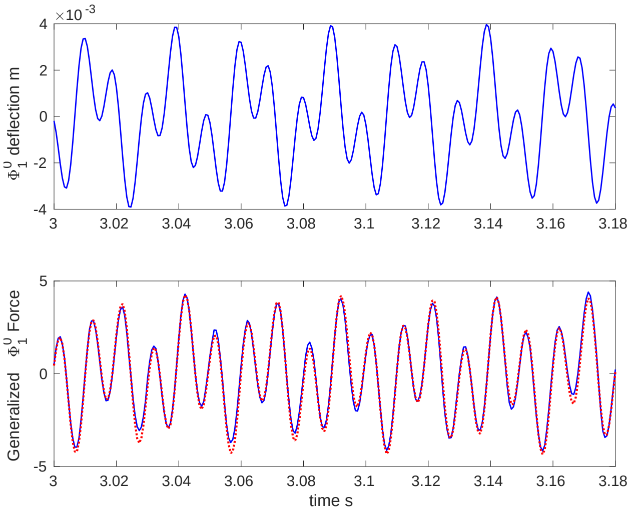

Figure 7: Rational-Matrix Approximation time domain validation, comparison of the simulated and reconstructed first collective mode generalised force for an arbitrary first flapping collective mode; blue line in the output represents the LL simulated load whereas the red dashed line is the RMA reconstructed.

RMA of the aerodynamic matrix is used in the system of Eq. (11), and the rotor aeroelastic analysis is performed, Fig. 8 depicts the poles for the rotor at a pitch angle of $6°$. In the box inside the figure the critical eigenvalue is highlighted, looking at its frequency it is possible to identify it as a lead-lag pole ($f \simeq 25Hz$).

This figure also shows the poles obtained with the two subsystems one can define considering the only collective or differential variable and the corresponding aerodynamic, as shown in the figure the critical poles coming from the different models are almost the same. Then the sensitivity of the rotor's aeroelastic stability to the pitch angle variation is assessed. Specifically, the RMA of the aerodynamic matrix at different pitch angles is performed, and the corresponding system poles are evaluated. The root locus varying the pitch angle is depicted in Figure 9, which shows the stabilizing effect of the aerodynamics as the pitch angle increases. Note that, to make the figure clear, exploiting the outcomes of the previous analysis, only the collective poles are depicted.

Finally, Fig. 10 shows the comparison between the experimentally evaluated lead-lag damping coefficients and the ones obtained with the herein pro-

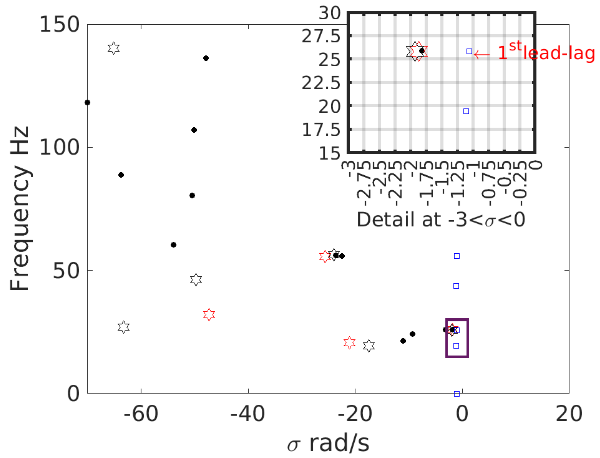

Figure 8: Poles of the complete linearised aeroelastic system, $\theta_C = 6°$; black dots are for the complete system, red stars for the collective subsystem and blue stars for the differential one. Finally, blue squares represent the structural poles without aerodynamics.

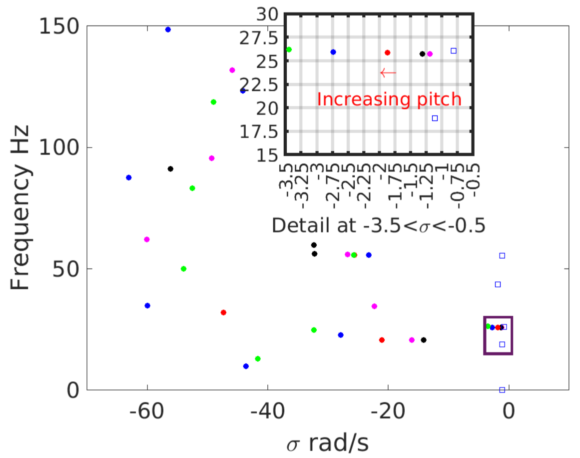

Figure 9: Root locus of the aeroelastic system varying the pitch angle.

posed technique. The figure also reports the theoretical prediction, provided directly by Sharpe in its paper, based on the Hodges and Dowell work (Ref. 1, 28) as well as the results obtained with a commercial code. There is a very good agreement between the numerical and experimental results and, moreover, from an engineering point of view, the numerical results are always conservative, slightly underestimating the experimental damping coefficient. On the other hand, standard and classic theoretical prediction tends to overestimate the lead-lag damping of the rotor, whereas the commercial code results stand in the middle (between theoretical and experimental), in particular for high values of collective pitch angles.

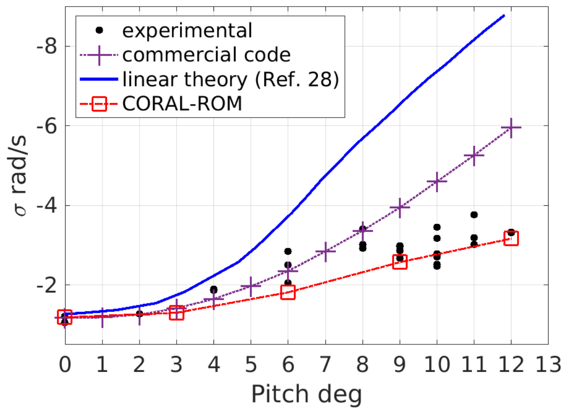

Figure 10: Comparison between experimental (Ref. 11), commercial code, theoretical (Ref. 28) and numerical evaluated lead-lag damping coefficients.

6. CONCLUSIONS

A novel technique for the assessment of the aeroelastic stability of a rotor has been proposed and successfully applied to the two-bladed hovering rotor experimentally analysed by Sharpe in 1986. Starting from the numerical simulation of the rotor the unsteady aerodynamic has been linearised, identified and its reduced order representation obtained, the aerodynamic reduced order model coupled with the linearised structural system and the aeroelastic stability was assessed by solving the associated eigenproblem. The accuracy of the proposed method is proven by the comparison with the experimentally measured lead-lag damping coefficients. In this work, a medium-fidelity solver based on the lifting line theory has been adopted to evaluate the aerodynamic load, but, depending on the available computational capacity, the aerodynamic modelling of the problem can be arbitrarily implemented and improved without changing the proposed procedure. In the next future, the proposed technique will be extended to rotors in forward flight and applied to different and more complex rotor configurations (droop angle, pre-cone, *etc.*).

REFERENCES

1. D. H. Hodges and E. H. Dowell, "Nonlinear equation for the elastic bending and torsion of twisted nonuniform rotor blades," Tech. Rep. TN D-7818, NASA, 1974.
2. D. Petot, "Differential equation modeling of dynamic stall," *La Recherche Aerospatiale*.

3. V. Truong, "A 2-d dynamic stall model based on a hopf bifurcation," in *18th European Rotorcraft Forum, ERF*, 1993.
4. M. Gennaretti, A. Corbelli, and F. Mastroddi, "A comparison among some aeroelastic models for the stability analysis of a flap-lag-torsion helicopter rotor in hover," in *EUROPEAN ROTORCRAFT FORUM*, vol. 26, pp. 68–68, AAAF; 1998, 2000.
5. M. Gennaretti and L. Greco, "Whirl flutter analysis of prop-rotors using unsteady aerodynamics reduced-order models," *The Aeronautical Journal*, vol. 112, no. 1131, pp. 233–242, 2008.
6. M. Gennaretti and D. Muro, "Multiblade reduced-order aerodynamics for state-space aeroelastic modeling of rotors," *Journal of Guidanceircraft*, vol. 49, no. 2, pp. 495–502, 2012.
7. F. Nitzsche, C. Spieß, R. Leibbrandt, M. Gennaretti, G. Bernardini, J. Serafini, V. Riziotis, G. Papadakis, N. Spyropoulos, A. Siami, D. Hilewit, and M. Rafiee, "A new comprehensive analysis tool for the preliminary design and design evaluation of helicopters - the coral project," in *47th European Rotorcraft Forum, United Kingdom*, 7-9th September 2021.
8. C. Pasquali, J. Serafini, R. Gori, R. Leibbrandt, and M. Gennaretti, "Algorithm for identification of helicopter open-loop transfer functions and reduced-order modeling," in *37th European Rotorcraft Forum, ERF*, 2022.
9. R. Gori, F. Pausilli, M. D. Pavel, and M. Gennaretti, "State-space rotor aeroelastic modeling for real-time helicopter flight simulation," in *Advanced Materials Research*, vol. 1016, pp. 451–459, Trans Tech Publ, 2014.
10. M. Gennaretti, C. Pasquali, F. Cardito, J. Serafini, G. Bernardini, and R. Celi, "Dynamic wake inflow modeling in ground effect for flight dynamics applications," in *AHS 73nd Annual Forum & Technology Display*, 2017.
11. D. L. Sharpe, "An experimental investigation of the flap-lag-torsion aeroelastic stability of a small-scale hingeless helicopter rotor in hover," tech. rep., 1986.
12. R. Gori, J. Serafini, M. Molica Colella, and M. Gennaretti, "Assessment of a state-space aeroelastic rotor model for rotorcraft flight dynamics," *CEAS Aeronautical Journal*, vol. 7, no. 3, pp. 405–418, 2016.
13. S. G. Voutsinas, "Vortex methods in aeronautics: How to make things work," *International Journal Computational Fluid Dynamics*, vol. 20.
14. L. Prandtl, "Applications of modern hydrodynamics to aeronautics," tech. rep., 1925.
15. W. F. Phillips and D. O. Snyder, "Modern adaptation of prandtl's classic lifting-line theory," *Journal of Aircraft*, vol. 37, no. 4, p. 662–670, 2000.
16. S. G. Voutsinas and D. G. Triantos, "High resolution aerodynamic analysis of full helicopter configurations," 1999.
17. L. Morino, "A General Theory of Unsteady Compressible Potential Aerodynamics," *NASA CR-2464*, Dicembre 1974.
18. K. Wang, V. A. Riziotis, and S. G. Voutsinas, "Aeroelastic stability of idling wind turbines," *Wind Energy Science*, vol. 2, no. 2, pp. 415–437, 2017.
19. G. Papadakis, *Development of a hybrid compressible vortex particle method and application to external problems including helicopter flows*. PhD thesis, National Technical University of Athens, 2015.
20. N. Spyropoulos, G. Papadakis, J. M. Prospathopoulos, and V. A. Riziotis, "Investigating the level of fidelity of an actuator line model in predicting loads and deflections of rotating blades under uniform free-stream flow," *Applied Sciences*, vol. 11, no. 24, p. 12097, 2021.
21. S. Zafeiris, "The overset grid assembly (chimera) of unstructured partitioned grids coupled with the artificial compressibility roe solver and applications in marine hydrodynamics," 2023.
22. T. Andronikos, "Hovering helicopter interaction with the ground and bluff bodies: A cfd based investigation," 2022.
23. S. G. Huberson and S. G. Voutsinas, "Particles and grid," *Computers & fluids*, vol. 31, no. 4-7, pp. 607–625, 2002.
24. T. Bagherpour, X. Li, D. Manolas, and V. Riziotis, "Modeling of material bend-twist coupling on wind turbine blades," *Composite Structures*, vol. 193, pp. 237–246, 2018.
25. D. Manolas, V. Riziotis, and S. Voutsinas, "Assessing the importance of geometric nonlinear effects in the prediction of wind turbine blade loads," *Journal of Computational and Nonlinear Dynamics*, vol. 10, no. 4, p. 041008, 2015.
26. J. S. Bendat and A. G. Piersol, *Random data analysis and measurement procedures*. IOP Publishing, 2000.
27. Z. Bohdanecký, P. Lánský, and T. Radil, "An integral measure of the coherence function between pairs of eeg recordings," *Electroencephalography and Clinical Neurophysiology*, vol. 54, no. 5, pp. 587–590, 1982.
28. D. Hodges and R. Ormiston, "Stability of elastic bending and torsion of uniform cantilever rotor blades in hover with variable structural coupling," NASA Technical Note TN D-8192, NASA, 1976.